Viscomagnetic Heat Flux Experiments as a Test of Gas Kinetic Theory in the Burnett Regime

G. E. J. Eggermont*, P. W. Hermans, L. J. F. Hermans, H. F. P. Knaap, and J. J. M. Beenakker

Huygens Laboratorium der Rijksuniversiteit Leiden, Leiden, The Netherlands

Z. Naturforsch. **33a**, 749–760 (1978); received March 22, 1978

Dedicated to prof. dr. L. Waldmann on the occasion of his 65th birthday

In a rarefied polyatomic gas streaming through a rectangular channel, an external magnetic field produces a heat flux perpendicular to the flow direction. Experiments on this "viscomagnetic heat flux" have been performed for CO, N_2, CH_4 and HD at room temperature, with different orientations of the magnetic field. Such measurements enable one to separate the boundary layer contribution from the purely bulk contribution by means of the theory recently developed by Vestner. Very good agreement is found between the experimentally determined bulk contribution and the theoretical Burnett value for CO, N_2 and CH_4, yet the behavior of HD is found to be anomalous.

1. Introduction

The application of an external magnetic field has proven to be a valuable tool in the studies of the transport properties of polyatomic gases. It yields information on the non-sphericity of the molecules and provides a test of the kinetic theory in the dilute gas regime. This "Senftleben-Beenakker effect" has been extensively studied over the last decade, both experimentally and theoretically, for dilute polyatomic gases and for mixtures of polyatomic and noble gases [1].

In the case of rarefied gases a magnetic field seems to be an even more powerful tool since effects, predicted by kinetic theory but — in the field free case — inaccessible to experimental verification, can be studied if an external magnetic field is applied; an example of such an effect is the subject of this paper. In a rarefied gas second order spatial derivatives of the velocity produce a heat flux, as noted already by Maxwell [2]. This coupling between viscous flow and heat flux has been inaccessible to experimental investigation because the heat flux occurs in the same direction as the flow velocity of the gas and is overwhelmed by much larger effects, such as the expansion of the gas. In a rarefied gas consisting of polyatomic molecules, however, the application of an external magnetic field gives rise to a transverse heat flux perpendicular to the flow direction. Such a transverse heat flux is much easier to investigate. This "viscomagnetic heat flux" was predicted by Levi, McCourt and Beenakker [3] and its phenomenological expression reads for a set up as given in Fig. 1:

$$q_y = L_{yxzz}(\boldsymbol{H}) \frac{\partial^2 v_x}{\partial z^2}, \tag{1}$$

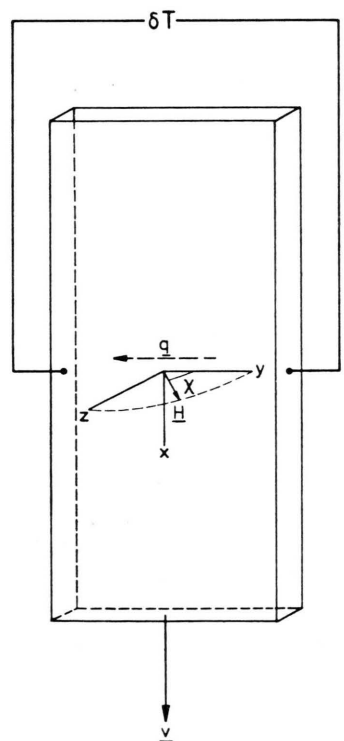

Fig. 1. Schematic diagram of the apparatus for the measurement of the viscomagnetic heat flux. The direction of the heat flux indicated is that observed for N_2.

* Present address: Philips Research Laboratories, Department Amsterdam, Oosterringdijk 18, Amsterdam, The Netherlands.

where q_y is the viscomagnetic heat flux, v_x is the flow velocity, $L_{yxzz}(\boldsymbol{H})$ is the (field dependent) coupling coefficient and $\boldsymbol{H}$ is the magnetic field, $\boldsymbol{H} = H\boldsymbol{h}$, $\boldsymbol{h} \cdot \boldsymbol{h} = 1$.

In the stationary situation the viscomagnetic heat flux q_y, which will be denoted as q when no confusion can arise, causes a small temperature difference δT across the channel.

Preliminary results on the viscomagnetic heat flux were reported for N_2 in a previous paper [4]. In this paper the experiment will be described in more detail and results for the gases CO, N_2, CH_4 and HD at room temperature will be given. Data will be reported for the effect at different orientations of the field. Such a study of the angular dependence is quite useful, since it provides a more sensitive test for the validity of the theory. The theoretical description of this effect has been given by Vestner [5], who included both the contributions originating in the bulk of the gas (given already by Levi et al. [3]) and the contributions arising from boundary layer effects. The experimental results will be compared with Vestner's theory.

2. Experimental

2.1. Apparatus and Calibration Procedure

The experiments were performed with a rectangular channel, schematically drawn in Figure 1. The length of the channel is 80 mm, the width is 10 mm and the thickness is 1.0 mm. The channel walls are made of low thermal conductance polyester "mylar", of thickness 75 μm. The transverse heat flux caused by the viscous flow in the magnetic field produces a small temperature difference δT (of the order 10^{-3} K) across the channel. This temperature difference is detected with two thermistors, glued to the narrow walls of the channel. These thermistors (Philips manufactured beads of approximately 0.5 mm diameter, having a resistance of 20 kΩ at room temperature) are part of a Wheatstone bridge circuit and the field induced unbalance of the bridge is, in steady state, proportional to the heat flux. For calibration purposes the heat flux can be simulated by electrically heating one of the two narrow walls. To this end, both narrow walls were lined on the inside with heating strips. These heaters consist of mylar strips (1 mm wide, 80 mm long and 15 μm thick) coated with a thin layer (5 nm) of aluminum, having a resistance of approximately 500 Ω. Calibration is obtained by electrically producing a well defined heat input in one of the channel walls and observing the resulting temperature difference across the channel in the stationary state. The interpretation of this calibration is not trivial, since the opposite narrow wall is not a heat sink. As a result, in such a symmetric arrangement, the field-induced heat flux q must be derived from the corresponding temperature difference δT with the use of the formula

$$q = \frac{1}{2} \frac{q_{\mathrm{cal}}}{\delta T_{\mathrm{cal}}} \delta T$$

where $q_{\mathrm{cal}} = i^2 R/A$ is the calibration heat flux, with i the current through the heater, R the heater resistance and A the area of the heated wall (80 mm × 1 mm), while δT_{cal} is the temperature difference observed during calibration. The factor 1/2 * can be readily found from the electric circuit analog. It can also be explained heuristically by noting that, in the actual measurement, the field induced heat flux heats one wall and simultaneously cools the other one by the same amount.

The validity of the above relation was confirmed experimentally by performing one additional measurement and calibration with one of the narrow walls brought into good thermal contact with a brass heat sink over its entire length. In this case, the formula $q = (q_{\mathrm{cal}}/\delta T_{\mathrm{cal}})\delta T$ was used, and the earlier result for the viscomagnetic heat flux q was reproduced within experimental error. Apart from this one measurement, all results were obtained without the use of a heat sink, which by virtue of its removing the symmetry of the setup, creates additional thermal instabilities.

A radiation shield is placed around the channel to cut down heat losses. The channel is placed inside a vacuum jacket, which in turn is placed in a dewar with a non-circulating waterbath. It is possible to detect temperature differences between the two thermistors as small as 2×10^{-5} K. The gas flow through the channel is stabilized with a Moore constant-differential type flow controller (model 63 SD-L). Separate leads are used to measure the pressure at the entrance and the exit of the channel.

* Unfortunately, this factor of ½ had been overlooked in the presentation of the preliminary results (Ref. [4]). Consequently, the experimental results given in Ref. [4] are too large by a factor of 2.

2.2. *Checks on the Apparatus*

With N_2 as a test gas, a few tests on the apparatus were carried out. First, it was verified that the effect is odd in the field direction. Furthermore the effect was found to be proportional to the pressure drop Δp across the channel, for fixed values of mean pressure p and field strength H. Since Δp is proportional to $\partial^2 v_x/\partial z^2$ through the Navier Stokes equation $\nabla p = 2\eta\,\nabla \cdot \overline{\nabla v}$, this is in agreement with Equation (1).

A transverse pressure gradient $\partial p/\partial y$ will occur due to the magnetic field effect on the viscosity [6]. This could be a source of error: since the bridge current heats the thermistors somewhat above ambient temperature pressure changes in the gas near the thermistor can, through the Knudsen effect on the thermal conductivity, produce changes in the temperature of the thermistors. To estimate the error due to this effect, we measured the viscomagnetic heat flux for N_2 ($H = 4.5$ kOe, $p = 0.95$ torr) using different voltages over the Wheatstone bridge: 0.5 V, 1.0 V, 1.5 V, 3.0 V, corresponding to heat inputs in the thermistors in the ratio 1:4:9:36. Only at the highest power a decrease of about 10% in the effect was observed. As the measurements of the viscomagnetic heat flux were performed with a voltage over the bridge of 0.5 V or 1.0 V we can safely assume that the influence of the transverse momentum transport was well below 1% and thus negligible.

Another error source is the fact that the channel may be deformed somewhat by the pressure of the gas inside. In order to estimate this effect, the flow resistance was measured for various overpressures in the channel relative to the vacuum jacket, which was open to atmospheric pressure in this test. We compared the pressure drop along the channel with the pressure drop along a standard capillary, placed in series with the channel. The flow resistance at an overpressure of 4 torr was found to be about 10% smaller than at 0.5 torr. This means that the average thickness of the channel has increased from 1.0 mm to about 1.03 mm. Since such an increase does not affect the value of $\nabla\nabla v$ for a given Δp, the value of q_y will not be affected. However, during the calibration a width of 1.0 mm is heated, to simulate a viscomagnetic heat flux generated over an effective width of 1.03 mm. As the measurement of the viscomagnetic heat flux were mostly performed at an average pressure of 0.5—2 torr the error due to the deformation of the channel is estimated to be about 1%. This error has been neglected.

2.3. *Knudsen Corrections*

At high pressures, the value of $(q/\Delta p)_{\max}$ was, as should be expected, found to be inversely proportional to the pressure. Therefore the quantity $pq/\Delta p$ is plotted vs. H/p as shown for N_2 in Figure 2.

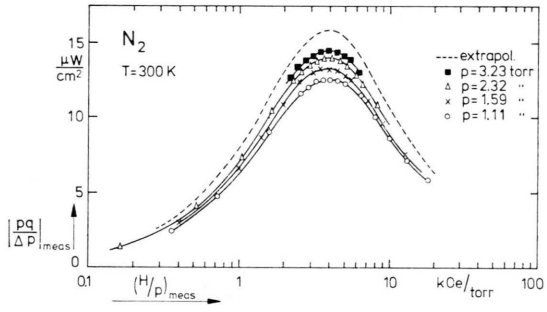

Fig. 2. The viscomagnetic heat flux as measured for N_2 at 300 K at $\chi = \pi/2$. The dotted line is an extrapolation to zero mean free path.

It is seen that at low pressures, where the mean free path is not small compared to the dimensions of the apparatus, the measured $pq/\Delta p$ values decrease due to Knudsen effects. A standard technique for Knudsen corrections was used [6, 7] to extrapolate to a mean free path negligibly small compared to the apparatus dimensions. It is assumed that the correction can be applied with

$$(pq/\Delta p) = (pq/\Delta p)_{\text{meas}}(1 + K_{\text{mag}}/p)\,, \qquad (2)$$

where $(pq/\Delta p)$ is the value, corresponding to zero mean free path, and K_{mag} is a Knudsen coefficient. According to Eq. (2) a plot of $[|pq/\Delta p|_{\text{meas, max}}]^{-1}$ vs. $1/p$ should give a straight line. For N_2 such a

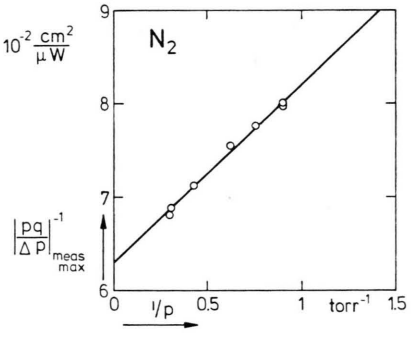

Fig. 3. Determination of the Knudsen coefficient K_{mag} from the maximum of the effect at $\chi = \pi/2$.

plot of data, taken at $\chi = \pi/2$, is shown in Figure 3; from the slope the value of K_{mag} is found.

Similarly, the measured value of H/p for which the maximum occurs shows, at low pressures, a shift towards higher H/p values. The measured values, $(H/p)_{\text{meas}}$ are corrected for this Knudsen effect with

$$(H/p) = (H/p)_{\text{meas}}(1 + K_{\text{pos}}/p)^{-1}, \qquad (3)$$

where the Knudsen coefficient K_{pos} is determined from the slope of a plot of $(H/p)_{\text{meas, max}}$ vs. $1/p$. For N_2 such a plot is shown in Figure 4; K_{pos} is found to be negligibly small for this gas.

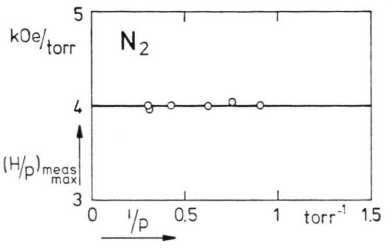

Fig. 4. Determination of the Knudsen coefficient K_{pos} from the position of the maximum of the effect at $\chi = \pi/2$.

The values of K_{mag} and K_{pos} for the various gases studied are given in Table I. To obtain numbers n, which are independent of the dimension of the apparatus we write $K/p = n\xi/t$, where ξ is the kinetic mean free path given by

$$\xi = \tfrac{2}{5}\sqrt{2}\,\eta\, p^{-1}(16 k_B T/\pi m)^{1/2}$$

and $t = 1.0$ mm is the thickness of the channel, η is the viscosity, k_B is Boltzmann's constant and m is the molecular mass. Values for n_{mag} and n_{pos} are listed in Table I.

Table I. Knudsen corrections for the viscomagnetic heat flux, determined at $\chi = \pi/2$.

	K_{mag} (torr)	K_{pos} (torr)	n_{mag}	n_{pos}
CO	0.23	0.0	5	0
N_2	0.30	0.0	6	0
CH_4	0.16[5]	0.16	4	4
HD	0.70	1.25	7	13

At all angles χ Knudsen corrections were applied with the use of the Knudsen coefficients, determined at $\chi = \pi/2$. This may not be entirely correct since the position of the maximum on the H/p-axis is determined by two different precession angles (see appendix), both having their own Knudsen behavior. Since the relative importance of the two precession angles depends somewhat on the angle χ, different values for K_{pos} can be expected. However, the changes are estimated to be small (see appendix). Experimental justification lies in the fact that the values found at $\chi = \pi/2$ make different pressure runs also coincide at the other angles.

3. Experimental Results

The viscomagnetic heat flux has been measured at room temperature for the gases CO, N_2, CH_4

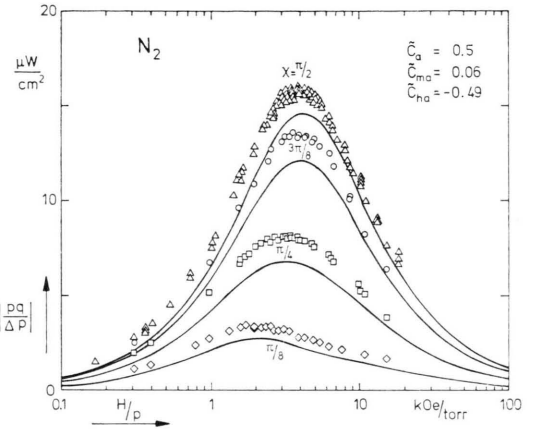

Fig. 5. Knudsen corrected results for N_2, for the angles $\chi = \pi/2, 3\pi/8, \pi/4$ and $\pi/8$. Pressures are between 1.02 and 3.23 torr. The theoretical curves correspond to Equation (7).

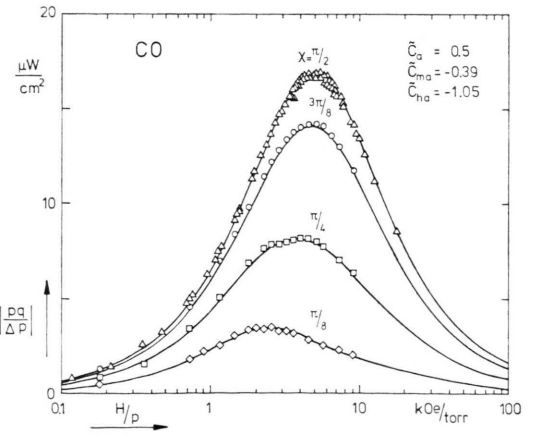

Fig. 6. Knudsen corrected results for CO, for the angles $\chi = \pi/2, 3\pi/8, \pi/4$ and $\pi/8$. Pressures are between 1.15 and 3.40 torr. The theoretical curves correspond to Equation (7).

and HD. The purity of the gases was better than 99.9% for CO and N_2 and better than 99.8% for CH_4. The HD gas was manufactured by Carl Roth and subsequently fractionally distilled at 20 K, to a purity of better than 96% HD, about 3% D_2 and less than 1% H_2. A better purity could have been obtained, but this was thought to be unnecessary. The effect was studied at five different angles $\chi = \pi/2$, $3\pi/8$, $\pi/4$, $\pi/8$, and 0 (see Figure 1). At the angle $\chi = 0$ no effect is observed. Results of these measurements, after Knudsen corrections have been applied, are given in Figs. 5—8, and summarized in Table II. The direction of the heat flux for N_2 is indicated in Figure 1. For CO the same direction is observed, whereas for CH_4 and HD the effect has the opposite direction; this is a consequence of the fact that N_2 and CO have a negative molecular g-factor, while CH_4 and HD have a positive g-factor.

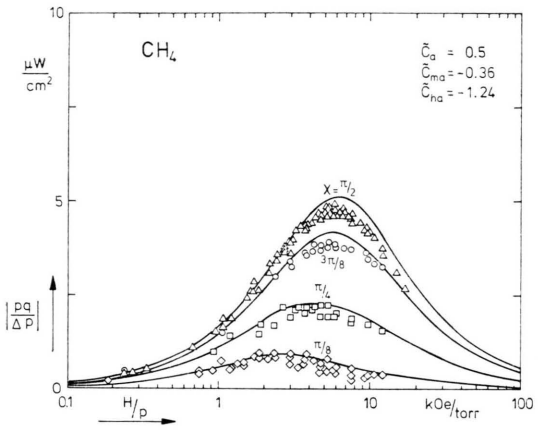

Fig. 7. Knudsen corrected results for CH_4, for the angles $\chi = \pi/2$, $3\pi/8$, $\pi/4$ and $\pi/8$. Pressures are between 1.03 and 2.77 torr. The theoretical curves correspond to Equation (7).

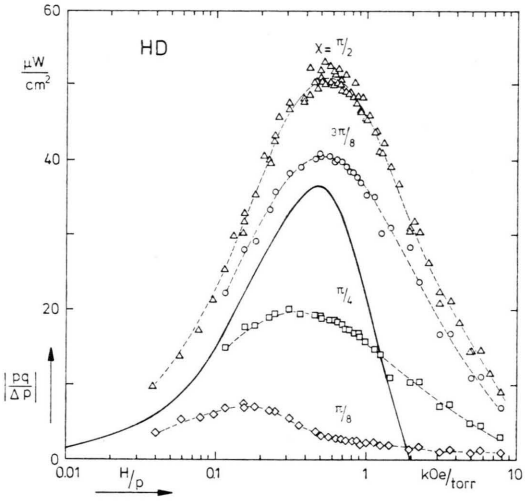

Fig. 8. Knudsen corrected results for HD, for the angles $\chi = \pi/2$, $3\pi/8$, $\pi/4$ and $\pi/8$. Pressures are between 1.31 and 2.93 torr. The dotted lines are smooth curves through the experimental points. The solid line is the theoretical curve for $\chi = \pi/2$ which corresponds to Eq. (7) with $\tilde{C}_a = 0.5$, $\tilde{C}_{ma} = -0.83$ and $\tilde{C}_{ha} = -1.18$. Similar discrepancies occur for other values of χ (not shown).

Table II. Knudsen corrected results for CO, N_2, CH_4 and HD.

χ	CO		N_2		CH_4		HD	
	$\left(\frac{H}{p}\right)_{max}$ kOe/torr	$\left\|\frac{pq}{\Delta p}\right\|_{max}$ μW/cm²	$\left(\frac{H}{p}\right)_{max}$ kOe/torr	$\left\|\frac{pq}{\Delta p}\right\|_{max}$ μW/cm²	$\left(\frac{H}{p}\right)_{max}$ kOe/torr	$\left\|\frac{pq}{\Delta p}\right\|_{max}$ μW/cm²	$\left(\frac{H}{p}\right)_{max}$ kOe/torr	$\left\|\frac{pq}{\Delta p}\right\|_{max}$ μW/cm²
$\frac{\pi}{2}$	5.0	16.8	4.0	15.8	6.0	4.7	0.55	51
$\frac{3\pi}{8}$	4.8	14.2	3.8	13.5	5.5	3.8	0.5	40.5
$\frac{\pi}{4}$	3.9	8.2	3.4	8.1	4.5	2.2	0.35	20
$\frac{\pi}{8}$	2.3	3.6	1.9	3.4	3	0.9	0.2	7.5

4. Theory

Before going into the details of the theory of Vestner [5] we will show how symmetry arguments impose restrictions on the angular dependence of the viscomagnetic heat flux. The magnetic field $\boldsymbol{H}$ lies in the yz-plane (see Figure 1). For a set up as given in Fig. 1 one again writes the phenomenological relation between the viscomagnetic heat flux q_y and the driving force $\partial^2 v_x/\partial z^2$ as

$$q_y = L_{yxzz}(H_y, H_z, n_z)\frac{\partial^2 v_x}{\partial z^2}\,. \tag{1a}$$

The tensor element L_{yxzz} depends on the magnetic field components H_y, H_z, on the orientation of the surface denoted by the normal vector n_z, on the pressure, on the properties of the gas and on the gas-surface interaction. For simplicity, only the quantities essential for the angular dependence of the effect have been explicitly written in Equation (1a). The symmetry of the arrangement requires the relation (1a) to be invariant under the following transformations of the coordinate system:

inversion:

$$x, y, z, H_y, H_z, n_z \rightarrow -x, -y, -z, H_y, H_z, -n_z$$

and rotation by π around

the y-axis:

$$x, y, z, H_y, H_z, n_z \rightarrow -x, y, -z, H_y, -H_z, -n_z\,,$$

the z-axis:

$$x, y, z, H_y, H_z, n_z \rightarrow -x, -y, z, -H_y, H_z, n_z\,.$$

From the inversion invariance one obtains the requirement

$$L_{yxzz}(H_y, H_z, n_z) = L_{yxzz}(H_y, H_z, -n_z). \tag{4}$$

The rotation invariances lead to the requirements

$$L_{yxzz}(H_y, H_z, n_z) = -L_{yxzz}(H_y, -H_z, -n_z)\,, \tag{5a}$$

$$L_{yxzz}(H_y, H_z, n_z) = L_{yxzz}(-H_y, H_z, n_z)\,. \tag{5b}$$

Consequently, L_{yxzz} is even in n_z and $H_y = H\cos\chi$ and odd in $H_z = H\sin\chi$. Hence we can write because of symmetry requirements

$$L_{yxzz} = \sin\chi\, f(\cos^2\chi) = \sin\chi \sum_{p=0}^{\infty} \cos^{2p}\chi\, L_p(H)\,. \tag{6}$$

In the kinetic theory of the viscomagnetic heat flux Vestner has taken into account the bulk as well as the boundary layer contributions. The total heat flux is written as a sum of the bulk heat flux $\boldsymbol{q}_b$ and the "surface heat flux" $\boldsymbol{q}_s$. The boundaries manifest themselves in two ways: they influence the bulk heat flux $\boldsymbol{q}_b$ and they cause the surface heat flux $\boldsymbol{q}_s$, which accounts for the difference between the actual value of the heat flux at the wall and the value of $\boldsymbol{q}_b$ extrapolated to the wall. Essential is the behavior near the wall of the tensor polarization $\overline{\boldsymbol{JJ}}$ and the Kagan polarization $\boldsymbol{W}\overline{\boldsymbol{JJ}}$ (being the only two angular momentum dependent polarizations taken into account). Moment equations derived from the Waldmann-Snider equation are solved with appropriate boundary contributions. The boundary conditions are found from the entropy production at the walls by application of Waldmann's thermodynamical method. For details the reader is referred to the original article [5]. The final result for a set-up as in Fig. 1 is given by

$$\left|\frac{pq}{\Delta p}\right| = \sin\chi\,\frac{\lambda T}{l}\,[\delta + \Delta_1 + \cos^2\chi(\Delta_2 - 2\Delta_1)] \tag{7}$$

where the angle dependence is given explicitly and the field dependence enters through the quantities δ, Δ_1 and Δ_2. These are complicated functions of H/p and of effective cross sections which also occur in the Senftleben-Beenakker effects for dilute gases. Details can be found in Appendix I. The expression is in agreement with the general expression based on symmetry considerations of Equation (6). The fact that no higher powers in $\cos^2\chi$ occur than a $\cos^2\chi$ term, is related to the fact that only tensor polarizations of rank two in the angular momentum $\boldsymbol{J}$ (viz. $\overline{\boldsymbol{JJ}}$ and $\boldsymbol{W}\overline{\boldsymbol{JJ}}$) are taken into account. Experimental agreement with this structure will give a justification for this aspect of the theory. The quantity δ contains only pure bulk contributions, and in fact is apart from a constant factor the transverse thermal conductivity coefficient λ^{tr}. The quantities Δ_1 and Δ_2 are influenced by the boundary, and as such contain coefficients for the accommodation of the tensor polarization ($\tilde{C}_{\mathrm{a}}$) and for the production of the polarization at the boundary through a tangential force ($\tilde{C}_{\mathrm{ma}}$) and a tangential temperature gradient ($\tilde{C}_{\mathrm{ha}}$); furthermore the effective slip number ($\sigma + \alpha$) occurs, a quantity that describes thermal transpiration (an effect also present in monatomic gases).

A comparison of the experimental results with the theory has a twofold purpose. First of all, one wants to see in how far the experiment can be described by the theory and secondly one wants to determine the values for the hitherto unknown accomodation coefficients $\tilde{C}_{\ldots}$.

5. Analysis of the Experimental Results

In this section we will analyse the experimental results, presented in Sect. 3, in terms of Vestner's theory. The procedure of the analysis will be illustrated for CO. First it should be noted that the vanishing of the effect at $\chi = 0$ is in accordance with Equations (6) and (7). To obtain values for the adaptable parameters $\tilde{C}_a$, $\tilde{C}_{ma}$ and $\tilde{C}_{ha}$ we proceed as follows: With the data obtained for $\chi = \pi/2$, $3\pi/8$, $\pi/4$ and $\pi/8$, plots are made of $|pq/\Delta p|/\sin\chi$ vs. $\cos^2\chi$ for fixed H/p values; for some H/p values such plots are shown in Figure 9.

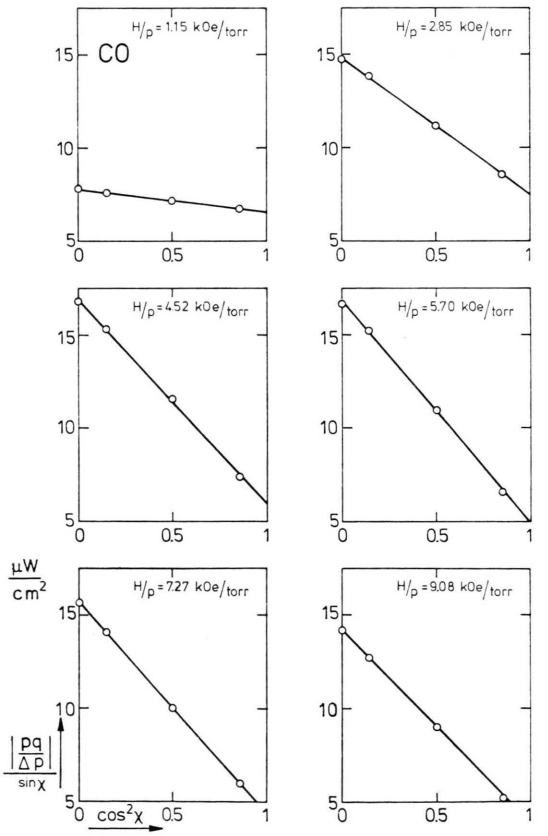

Fig. 9. Plots of $|pq/\Delta p|/\sin\chi$ vs $\cos^2\chi$ at various H/p values for CO.

As should be expected from Eq. (7), straight lines are found. This supports the assumption underlying Eq. (7) that only tensor polarizations up to rank two in angular momentum $\boldsymbol{J}$ are important. The straight line behavior is also an indirect test on the quality of the experimental data. The information contained in the lines is twofold: the slope of the line gives $(\lambda T/l)(\Delta_2 - 2\Delta_1)$ for the particular H/p value, and is strongly dependent on the values of $\tilde{C}_a$, $\tilde{C}_{ma}$ and $\tilde{C}_{ha}$. The intercept gives $(\lambda T/l)(\delta + \Delta_1)$ — the effect at $\chi = \pi/2$ — for that H/p value.

We now plot the slopes of the lines as a function of H/p (see Figure 10). Values of the parameters $\tilde{C}_a$, $\tilde{C}_{ma}$ and $\tilde{C}_{ha}$ can now be found such that the theoretical curve $(\lambda T/l)(\Delta_2 - 2\Delta_1)$ vs. H/p gives a good description of the experimental points. The effective slip number $(\sigma + \alpha)$ is taken to be 0.2 (Maxwell's value) and the various cross sections, needed in the calculation, are taken from Reference [8]. The exact procedure of varying the parameters $\tilde{C}_a$, $\tilde{C}_{ma}$ and $\tilde{C}_{ha}$ to obtain the best fits is described in Appendix II. The combinations of $\tilde{C}_a$, $\tilde{C}_{ma}$ and $\tilde{C}_{ha}$ found are represented in Fig. 11 by a line in a 3-dimensional space, spanned up by $\tilde{C}_a$, $\tilde{C}_{ma}$ and $\tilde{C}_{ha}$. The values are listed in Table III. In Fig. 10 the theoretical curve for $-(\lambda T/l)(\Delta_2 - 2\Delta_1)$ vs. H/p for a particular combination of $\tilde{C}$-parameters from Table III is given, together with the experimental points. Excellent agreement is found. The

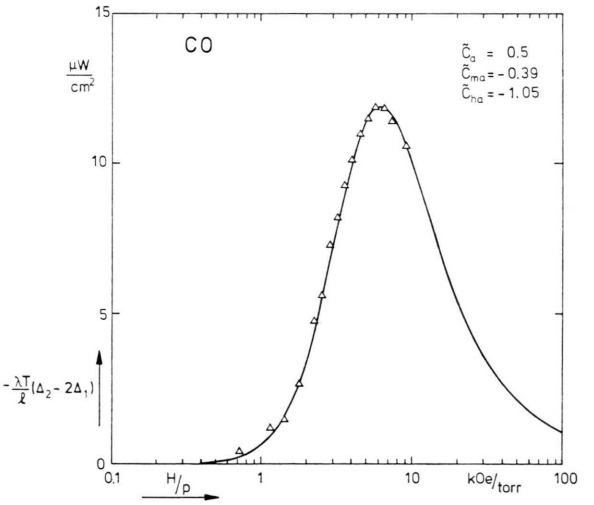

Fig. 10. The slopes of the straight lines as in Fig. 9 plotted as a function of H/p for CO. The theoretical curve $-(\lambda T/l)(\Delta_2 - 2\Delta_1)$ vs(H/p) is calculated with the parameters $\tilde{C}_a = 0.5$, $\tilde{C}_{ma} = -0.39$, $C_{ha} = -1.05$, $\sigma + \alpha = 0.2$.

theoretical curves found with the other combinations of $\tilde{C}$'s listed in Table III are indistinguishable from the one given in Figure 10.

The range of $\tilde{C}_a$ values, represented in Fig. 11 and Table III has been selected with the use of the Knudsen effects on the Senftleben-Beenakker effect for viscosity [6, 9, 10].

Table III. Combinations of $\tilde{C}_a$, $\tilde{C}_{ma}$ and $\tilde{C}_{ha}$ for CO, which give a good description of $-(\lambda T/l)(\Delta_2 - 2\Delta_1)$ vs(H/p) with the effective slip number $(\sigma+\alpha)=0.2$. The $\tilde{C}_a$-range is selected on the basis of the description of the Knudsen effects on the Senftleben-Beenakker effect for viscosity.

$\tilde{C}_a$	$\tilde{C}_{ma}$	$\tilde{C}_{ha}$
0.4	−0.65	−1.43
0.5	−0.39	−1.05
0.6	−0.13	−0.72
0.7	0.18	−0.36
0.8	0.47	−0.05
1.0	1.09	0.58

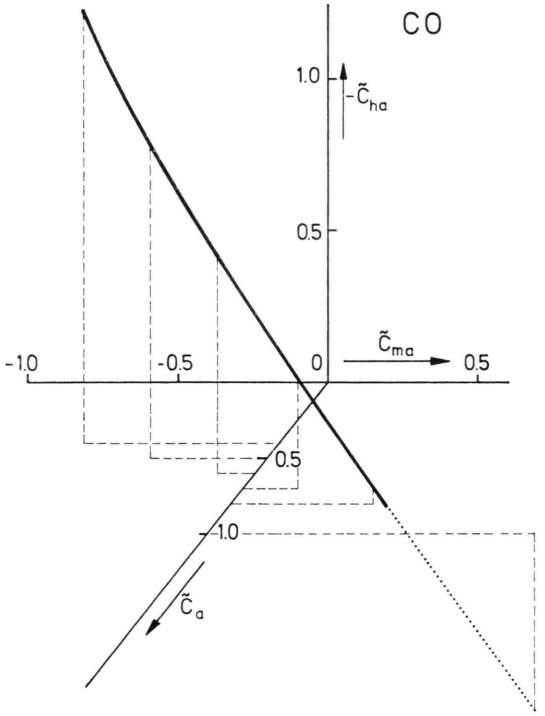

Fig. 11. Values of $\tilde{C}_a$, $\tilde{C}_{ma}$ and $\tilde{C}_{ha}$ which yield theoretical curves for $-(\lambda T/l)(\Delta_2 - 2\Delta_1)$ vs (H/p), that are indistinguishable from the one given in Figure 10. Only those combinations have been displayed which are compatible with the Knudsen corrections on the Senftleben-Beenakker effect for the viscosity.

We will now discuss the intercepts of the straight lines, $(\lambda T/l)(\delta + \Delta_1)$, which are the viscomagnetic heat flux results at $\chi = \pi/2$. The various sets of $\tilde{C}_a$, $\tilde{C}_{ma}$ and $\tilde{C}_{ha}$ which give the same $\Delta_2 - 2\Delta_1$ vs. H/p curves, give — because of the structure of the Δ_1 and Δ_2 expressions — also indistinguishable curves for Δ_1 vs. H/p curve. Since δ does not depend on the parameters $\tilde{C}$.. the experimental results at $\chi = \pi/2$ cannot be used to further narrow the range of $\tilde{C}$-parameters. We can use these results, however, as a test on the δ term in Equation (7). The theoretical expression for this δ term (see Appendix I), which accounts for the pure bulk (Burnett) effect, is used in combination with cross sections determined in other experiments to generate the theoretical curves in Figure 6. It is evident that very good agreement is found and that the Burnett theory is thereby confirmed.

As mentioned before, it is not possible to select a unique set of parameters $\tilde{C}_a$, $\tilde{C}_{ma}$ and $\tilde{C}_{ha}$ from experimental data, available at this time. Hopefully, future data on the birefringence in a rarefied polyatomic gas near the wall in the presence of a temperature gradient, determined by $\tilde{C}_a$ and $\tilde{C}_{at}$, will further narrow the $\tilde{C}_a$ range. The parameter $\tilde{C}_{at}$ is a surface coefficient, relating the production of $\overline{JJ}$-polarization near the wall to an incoming heat flux. Results of a similar analysis for N_2 are summarized in Figs. 12 and 5 and Table IV, and for

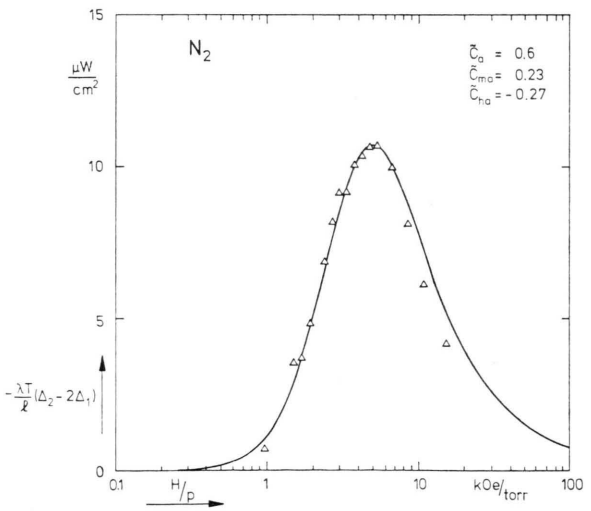

Fig. 12. The slopes of the straight lines as in Fig. 9 plotted as a function of H/p for N_2. The theoretical curve $-(\lambda T/l)(\Delta_2 - 2\Delta_1)$ vs (H/p) is calculated with the parameters $\tilde{C}_a = 0.6$, $\tilde{C}_{ma} = 0.23$, $\tilde{C}_{ha} = -0.27$, $\sigma + \alpha = 0.189$.

Table IV. Combinations of $\tilde{C}_a$, $\tilde{C}_{ma}$ and $\tilde{C}_{ha}$ for N_2, which give a good description of $-(\lambda T/l)(\Delta_2 - 2\Delta_1)$ vs(H/p), with the effective slip number $(\sigma + \alpha)$ taken 0.189. The $\tilde{C}_a$-range is selected on the basis of the description of the Knudsen effects on the Senftleben-Beenakker effect for viscosity.

$\tilde{C}_a$	$\tilde{C}_{ma}$	$\tilde{C}_{ha}$
0.1	−0.51	−1.46
0.2	−0.47	−1.27
0.3	−0.28	−0.96
0.4	−0.10	−0.71
0.5	0.06	−0.49
0.6	0.23	−0.27
0.7	0.43	−0.06
0.8	0.63	0.18
0.9	0.86	0.38
1.0	1.06	0.54

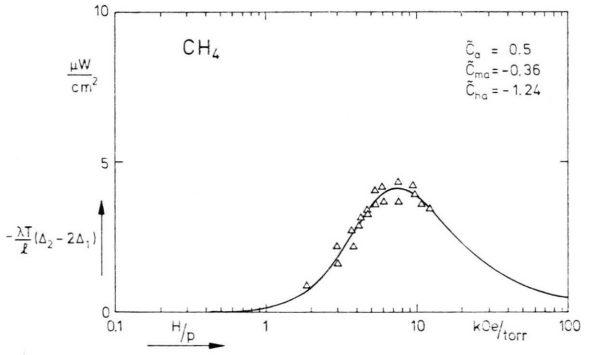

Fig. 13. The slopes of the straight lines as in Fig. 9 plotted as a function of H/p for CH_4. The theoretical curve $-(\lambda T/l)(\Delta_2 - 2\Delta_1)$ vs(H/p) is calculated with the parameters $\tilde{C}_a = 0.5$, $\tilde{C}_{ma} = -0.36$, $\tilde{C}_{ha} = -1.24$, $\sigma + \alpha = 0.2$.

Table V. Combinations of $\tilde{C}_a$, $\tilde{C}_{ma}$ and $\tilde{C}_{ha}$ for CH_4 which give a good description of $-(\lambda T/l)(\Delta_2 - 2\Delta_1)$ vs(H/p), with the effective slip number $(\sigma + \alpha) = 0.2$. The $\tilde{C}_a$-range is selected on the basis of the description of the Knudsen effects on the Senftleben-Beenakker effect for viscosity.

$\tilde{C}_a$	$\tilde{C}_{ma}$	$\tilde{C}_{ha}$
0.1	−0.91	−2.40
0.2	−0.84	−2.14
0.3	−0.71	−1.86
0.4	−0.53	−1.52
0.5	−0.36	−1.24
0.6	−0.20	−1.02
0.7	0.00	−0.80
0.8	0.19	−0.56
0.9	0.40	−0.34
1.0	0.62	−0.14
1.1	0.90	0.15
1.2	1.04	0.27

CH_4 in Figs. 13 and 7 and Table V. For N_2 the effective slip number $(\sigma + \alpha)$ is taken to be 0.189 [11]; for CH_4 the value 0.2 is chosen.

We will now discuss the results for HD. The experimental data do satisfy the symmetry requirements imposed by Equation (6). Straight lines are found if one plots $|pq/\Delta p|/\sin\chi$ vs. $\cos^2\chi$ at various H/p values, which means that the general structure of Eq. (7) is confirmed. This implies that the experiment supports also for HD the assumption made in the theory that no tensors of higher rank in $\boldsymbol{J}$ than rank two have to be considered. It is not possible, however, to obtain a good fit between the theoretical $-(\lambda T/l)(\Delta_2 - 2\Delta_1)$ curve and the experimental points by varying the parameters, as shown in Figure 14. The effective slip number $(\sigma + \alpha)$ is again taken to be 0.2. The theoretical curve is too narrow. It is not surprising, therefore that the $\chi = \pi/2$ curve cannot be fitted for HD.

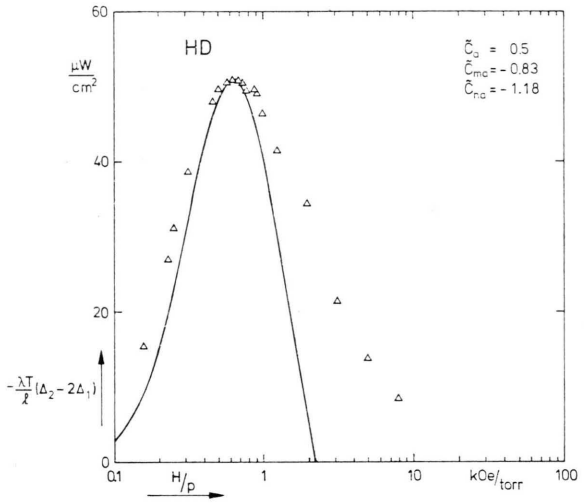

Fig. 14. The slopes of the straight lines as in Fig. 9 plotted as a function of (H/p) for HD. The theoretical curve $-(\lambda T/l)(\Delta_2 - 2\Delta_1)$ vs(H/p) is calculated with the parameters $\tilde{C}_a = 0.5$, $\tilde{C}_{ma} = -0.83$, $\tilde{C}_{ha} = -1.18$, $\sigma + \alpha = 0.2$.

It is clear that the theory cannot explain the experimental results for HD. This is not very surprising, since this theory has failed in the case of HD also for other low pressure effects, such as the thermomagnetic pressure difference [12] and the Knudsen effects on the flow birefringence [13, 14].

In summary, one remarks that the present experiments in combination with Vestner's theory

permit the boundary layer contribution to be separated experimentally from the pure bulk term δ. For this bulk term, very good agreement between experiment and theory is found for the gases CO, N_2 and CH_4. This is, to the authors' knowledge, the first time that a Burnett term in transport theory has been quantitatively verified.

With regard to the boudary layer contribution, only limited significance should be ascribed to the values of the adaptable parameters appearing in the theory, since no unique set of values has been determined by the experiments. The theory is seen to provide a poor description for the measurements for HD, a gas which has proven to be anomalous in several related experiments [12, 13, 14] as well.

Acknowledgements

Numerous discussions with Dr. H. Vestner are gratefully acknowledged. The authors are indebted to Mr. P. Zwanenburg for his expert construction of the apparatus.

This work is part of the research program of the "Stichting voor Fundamenteel Onderzoek der Materie (FOM)" and has been made possible by financial support from the "Nederlandse Organisatie voor Zuiver Wetenschappelijk Onderzoek (ZWO)".

Appendix I

In this appendix explicit expressions will be given for the quantities appearing in Eq. (7)

$$|pq/\Delta p| = \sin\chi(\lambda T/l)[\delta + \Delta_1 + \cos^2\chi(\Delta_2 - 2\Delta_1)] \tag{A.1}$$

where λ is the thermal conductivity of the gas, T is the temperature and l is the length of the channel. The functions δ and Δ_1, Δ_2 are given by

$$\delta = \tfrac{1}{2}\alpha\Psi_1[g(\xi_{12}) + 2g(2\xi_{12})] \tag{A.2}$$

and

$$\Delta_n = (\sigma+\alpha)\Psi^{(\eta)}\,g(n\,\xi_{02}) + \frac{r}{r-1}\Psi_2\,g(n\,\xi_{02}) - \frac{1}{r-1}\Psi_2\,g(n\,\xi_{12}) + \Psi_2\,\mathrm{Im}\left[\frac{\dfrac{1}{1+i\,n\,\xi_{02}} - \tilde{C}_{\mathrm{ma}}}{1+\tilde{C}_{\mathrm{a}}\sqrt{\dfrac{1+i\,n\,\xi_{02}}{1+i\,n\,\xi_{12}}}}\left(\frac{1}{1+i\,n\,\xi_{12}} + \tilde{C}_{\mathrm{ha}}\sqrt{\frac{1+i\,n\,\xi_{02}}{1+i\,n\,\xi_{12}}}\right)\right];\ n=1,2\,. \tag{A.3}$$

The function $g(\xi)=\xi/(1+\xi^2)$ gives the field dependence through the precession angles ξ_{02} and ξ_{12} ($\propto H/p$, the magnetic field strength to pressure ratio):

$$\xi_{pq} = \frac{\omega_{\mathrm{L}}}{n\,v_{\mathrm{rel}}\,\mathfrak{S}(p\,q)}\,,\quad v_{\mathrm{rel}} = \left(\frac{16\,k_{\mathrm{B}}\,T}{\pi m}\right)^{\frac{1}{2}}. \tag{A.4}$$

The precession angles are the ratio of the precession frequency $\omega_{\mathrm{L}} = g\,\mu_{\mathrm{N}}H/\hbar$ and a gas collision frequency; g is the rotational g-factor, μ_{N} is the nuclear magneton and H is the magnetic field strength. The quantity α is given by

$$\alpha = \frac{2}{5}\frac{\lambda_{\mathrm{transl}}}{\lambda}(1+\varepsilon) \tag{A.5}$$

where $\lambda_{\mathrm{transl}}$ is the translational part of the thermal conductivity and ε is a correction, which arises from the coupling through gas-gas collisions to higher moments. Typical values for gases like N_2 at room temperature are $\varepsilon \approx -0.1$, if the contribution from inelastic collisions is neglected. The combination $\sigma+\alpha$ appearing in Eq. (A.3) is the effective slip number found from thermal transpiration data [11] and is close to Maxwell's value 0.2. The quantities r, Ψ_1, Ψ_2 and $\Psi^{(\eta)}$ are in terms of effective cross sections given by

$$r = \frac{\mathfrak{S}(12)}{\mathfrak{S}(02)}\,,\quad \Psi_1 = f_1\Psi_0,\qquad \Psi_2 = \frac{2}{5}\frac{\lambda_{\mathrm{transl}}}{\lambda}\Psi_0\,,\quad \Psi^{(\eta)} = \frac{\mathfrak{S}^2\begin{pmatrix}20\\02\end{pmatrix}}{\mathfrak{S}(20)\,\mathfrak{S}(02)} \tag{A.6}$$

with

$$f_1 = \sqrt{\frac{4}{5}}\frac{\mathfrak{S}(02)}{\mathfrak{S}\begin{pmatrix}20\\02\end{pmatrix}} \cdot \left[\frac{-\mathfrak{S}\begin{pmatrix}1010\\1200\end{pmatrix}\mathfrak{S}(1001) + \mathfrak{S}\begin{pmatrix}1001\\1200\end{pmatrix}\mathfrak{S}\begin{pmatrix}1010\\1001\end{pmatrix}}{\mathfrak{S}(1010)\,\mathfrak{S}(1001) - \mathfrak{S}^2\begin{pmatrix}1010\\1001\end{pmatrix}}\right] \tag{A.7}$$

and

$$\Psi_0 = \sqrt{\frac{5}{4}}\,\frac{\mathfrak{S}\binom{20}{02}}{\mathfrak{S}(02)\,\mathfrak{S}(12)}\left[-\mathfrak{S}\binom{1010}{1200}+\mathfrak{S}\binom{1001}{1200}\frac{\mathfrak{S}\binom{1010}{1001}+\sqrt{\frac{2C_{\mathrm{rot}}}{5k_{\mathrm{B}}}}\,\mathfrak{S}(1010)}{\mathfrak{S}(1001)+\sqrt{\frac{2C_{\mathrm{rot}}}{5k_{\mathrm{B}}}}\,\mathfrak{S}\binom{1010}{1001}}\right] \tag{A.8}$$

where C_{rot} is the rotational heat capacity per molecule and k_{B} is Boltzmann's constant. The contribution to the heat flux in the bulk of the gas $\boldsymbol{q}_b$ which is completely determined by gas-gas collisions is given by Eq. (A.1) with δ as given in (A.2) and Δ_1, Δ_2 are given by

$$\Delta_n = \alpha\Psi^{(\eta)}\,g(n\,\xi_{02}) + \frac{r}{r-1}\,g(n\,\xi_{02}) - \frac{1}{r-1}\,\Psi_2\,g(n\,\xi_{12}); \quad n = 1, 2\,. \tag{A.9}$$

This result corresponds to that given by Levi et al. [3] for $\alpha = \frac{8}{5}\,\lambda_{\mathrm{transl}}/\lambda$ (i.e., $\varepsilon = 0$). The boundary layer influence on the heat flux in the bulk shows up in the expressions for Δ_1 and Δ_2, given in Eq. (A.3), viz. the term proportional to

$$1/(1 + i\,n\,\xi_{12})\,.$$

The contribution of the surface heat flux $\boldsymbol{q}_s$ is given in Eq. (A.3) by the term $\sigma\Psi^{(\eta)}\,g(n\xi_{02})$ and the term proportional to $\tilde{C}_{\mathrm{ha}}$.

Appendix II

Here we will describe the procedure that is used to obtain combinations of $\tilde{C}_{\mathrm{a}}$, $\tilde{C}_{\mathrm{ma}}$ and $\tilde{C}_{\mathrm{ha}}$, for which the theoretical curve $-(\lambda T/l)(\Delta_2 - 2\Delta_1)$ vs. H/p gives a good description of the experimental points (see Figure 10). The gas CO will be used as an example; the effective slip number $(\sigma+\alpha)$ for this gas is taken to be 0.2. With a fixed $\tilde{C}_{\mathrm{a}}$ value (e.g., $\tilde{C}_{\mathrm{a}} = 0.5$), the maximum value of the curve $-(\lambda T/l)(\Delta_2 - 2\Delta_1)$ and the position of the maximum on the H/p-axis is calculated as a function of $\tilde{C}_{\mathrm{ha}}$ for various $\tilde{C}_{\mathrm{ma}}$-values. The results are shown in Figures 15a and 15b.

By comparing the lines in Fig. 15a with the experimental value of

$$-(\lambda T/l)(\Delta_2 - 2\Delta_1)_{\max} = 11.9\ \mu\mathrm{W\ cm^{-2}},$$

we obtain pairs of values of the coefficients $\tilde{C}_{\mathrm{ma}}$ and $\tilde{C}_{\mathrm{ha}}$, which are represented in Figure 15c. In a similar way, Fig. 15b yields pairs of coefficients $\tilde{C}_{\mathrm{ma}}$ and $\tilde{C}_{\mathrm{ha}}$, which are also represented in Figure 15c. The coordinate of the point of intersection of the lines thus obtained, combined with the choosen value of $\tilde{C}_{\mathrm{a}}$, then yield a combination of $\tilde{C}_{\mathrm{a}}$, $\tilde{C}_{\mathrm{ma}}$ and $\tilde{C}_{\mathrm{ha}}$ for which the theoretical curve $-(\lambda T/l)(\Delta_2 - 2\Delta_1)$ vs. H/p has a maximum for which both magnitude and position are the same as the experimentally found values. This procedure is then repeated for other values of $\tilde{C}_{\mathrm{a}}$. In this way a whole set of combinations $\tilde{C}_{\mathrm{a}}$, $\tilde{C}_{\mathrm{ma}}$ and $\tilde{C}_{\mathrm{ha}}$ is found. The shape of the curves, determined by these combinations, turns out to be the same for all these combinations, and to fit the experimental results very well. The range for $\tilde{C}_{\mathrm{a}}$, presented in Fig. 11 and Table III, is selected on the grounds of

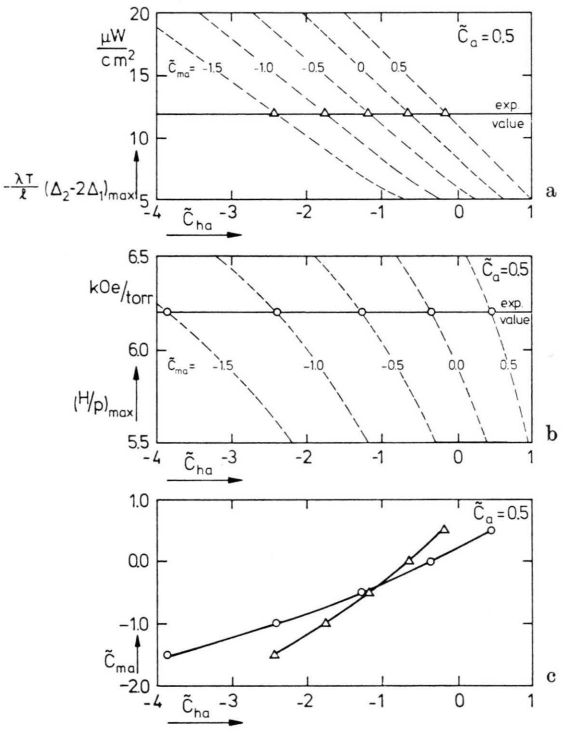

Fig. 15a—c. Theoretical curves for the maximum value $-(\lambda T/l)(\Delta_2 - 2\Delta_1)$ (Fig. a) and for the position of this maximum (Fig. b) for CO as a function of $\tilde{C}_{\mathrm{ha}}$ for various $\tilde{C}_{\mathrm{ma}}$ values; $\tilde{C}_{\mathrm{a}}$ is fixed. The values of $\tilde{C}_{\mathrm{ma}}$ and $\tilde{C}_{\mathrm{ha}}$ for which the theoretical curves intersect with the experimentally found values are displayed in Figure c.

the description of the Knudsen corrections on the Senftleben-Beenakker effect for viscosity. These Knudsen corrections are determined by the parameters $\tilde{C}_a$, $\tilde{C}_{ma}$ and C_m [10]) (the mechanical slip number $C_m = 1.2$ for CO). Since the experimentally obtained values for these corrections are not very accurate [6, 9], values of these coefficients, calculated with $\tilde{C}_a$ and $\tilde{C}_{ma}$ found in the analysis are thought to be acceptable if they are within 20% from the experimentally found Knudsen coefficient, describing the Knudsen effect on the magnitude of the effect, and within 50% of the value of the less reliable coefficient, describing the position of the effect.

[1] For a review see *e.g.*, J. J. M. Beenakker and F. R. McCourt, Ann. Rev. Phys. Chem. **21**, 47 (1970); J. J. M. Beenakker, Transport Properties in Gases in the Presence of External Fields, in Lecture Notes in Physics **31** (Springer Verlag, Berlin, 1974), p. 414.
[2] J. Cl. Maxwell, Phil. Trans. **170**, 231 (1879).
[3] A. C. Levi, F. R. McCourt, and J. J. M. Beenakker, Physica **42**, 363 (1969).
[4] G. E. J. Eggermont, P. W. Hermans, L. J. F. Hermans, and J. J. M. Beenakker, Phys. Letters **57A**, 29 (1976); L. J. F. Hermans, G. E. J. Eggermont, P. W. Hermans, and J. J. M. Beenakker, Progress in Astronautics and Aeronautics **51**, 695 (1977).
[5] H. Vestner, Z. Naturforsch. **31**a, 540 (1976).
[6] H. Hulsman, E. J. van Waasdijk, A. L. J. Burgmans, H. F. P. Knaap, and J. J. M. Beenakker, Physica **50**, 53 (1970).
[7] L. J. F. Hermans, J. M. Koks, A. F. Hengeveld, and H. F. P. Knaap, Physica **50**, 410 (1970).
[8] J. P. J. Heemskerk, G. F. Bulsing, and H. F. P. Knaap, Physica **71**, 515 (1974).
[9] H. Hulsman, F. G. van Kuik, K. W. Walstra, H. F. P. Knaap and J. J. M. Beenakker, Physica **57**, 501 (1972).
[10] H. Vestner, Z. Naturforsch. **29**a, 663 (1974).
[11] H. Vestner and L. Waldmann, Physica **86A**, 303 (1977).
[12] G. E. J. Eggermont, P. Oudeman, L. J. F. Hermans, and J. J. M. Beenakker, Physica, in press.
[13] F. Baas, J. N. Breunese, H. F. P. Knaap, and J. J. M. Beenakker, Physica **88A**, 1 (1977).
[14] H. Vestner, Z. Naturforsch. **29**a, 365 (1974).